

UIEDP: Underwater Image Enhancement with Diffusion Prior

Dazhao Du¹, Enhao Li¹, Lingyu Si^{2,3}, Fanjiang Xu^{2,*}, Jianwei Niu¹ and Fuchun Sun^{2,4}

¹Hangzhou Innovation Institute, Beihang University

²Institute of Software, Chinese Academy of Science

³University of Chinese Academy of Sciences

⁴Department of Computer Science and Technology, Tsinghua University

{dudazhao,lienhan,niujiangwei}@buaa.edu.cn, {lingyu,fanjiang}@iscas.ac.cn, fcsun@mail.tsinghua.edu.cn

Abstract

Underwater image enhancement (UIE) aims to generate clear images from low-quality underwater images. Due to the unavailability of clear reference images, researchers often synthesize them to construct paired datasets for training deep models. However, these synthesized images may sometimes lack quality, adversely affecting training outcomes. To address this issue, we propose UIE with Diffusion Prior (UIEDP), a novel framework treating UIE as a posterior distribution sampling process of clear images conditioned on degraded underwater inputs. Specifically, UIEDP combines a pre-trained diffusion model capturing natural image priors with any existing UIE algorithm, leveraging the latter to guide conditional generation. The diffusion prior mitigates the drawbacks of inferior synthetic images, resulting in higher-quality image generation. Extensive experiments have demonstrated that our UIEDP yields significant improvements across various metrics, especially no-reference image quality assessment. And the generated enhanced images also exhibit a more natural appearance.

1 Introduction

With the rise of marine ecological research and underwater archaeology, processing and understanding underwater images have attracted increasing attention. Due to the harsh underwater imaging conditions, underwater images usually suffer from various visual degradations, such as color casts, low contrast, and blurriness [Ancuti *et al.*, 2012; Ghani and Isa, 2015]. To enable advanced visual tasks like segmentation and detection of underwater images, underwater image enhancement (UIE) usually serves as a crucial preprocessing step [Islam *et al.*, 2020].

In recent years, deep learning-based methods have gradually outperformed traditional techniques in UIE. While many deep learning-based UIE models have been proposed [Li *et al.*, 2021; Guo *et al.*, 2023; Jiang *et al.*, 2023], they heavily rely on paired datasets for training. Due to the unavailability of clean reference images (also known as la-

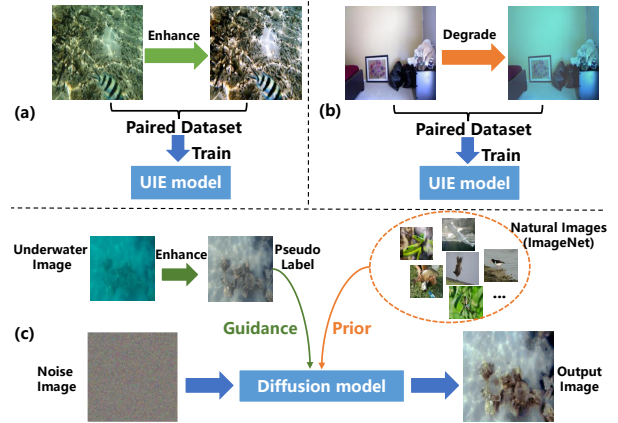


Figure 1: (a) Enhance real underwater images to obtain synthesized reference images, and construct paired samples for training UIE models. (b) Degrade natural images to obtain synthesized underwater images, and construct paired samples for training UIE models. (c) A diffusion model trained on ImageNet has natural image priors. To make full use of it, we guide the sampling process of the diffusion model with pseudo-labels generated by any UIE algorithm.

els) for real underwater scenes, researchers have employed various approaches to synthesize paired datasets. One approach involves employing multiple UIE algorithms to enhance each underwater image and manually selecting the visually optimal result as the reference image [Li *et al.*, 2019a; Peng *et al.*, 2023], as shown in Figure 1 (a). However, the upper limit of the reference image quality is limited by the chosen UIE algorithm. The alternative approach utilizes in-air images and corresponding depth maps to generate underwater-style images [Wang *et al.*, 2019; Li *et al.*, 2020], as shown in Figure 1 (b). Nevertheless, the synthesized underwater-style images are unreal since the exact degradation model is unknown. To address these issues, some studies have explored domain adaptation to bridge the domain gap between synthetic and real images [Chen and Pei, 2022; Wang *et al.*, 2023]. However, such methods often introduce additional discriminators for adversarial training, potentially leading to training instability and mode collapse. Additionally, there are unsupervised [Fu *et al.*, 2022] and semi-supervised [Huang *et al.*, 2023] approaches that either forgo

*Corresponding author.

the use of paired datasets or rely on limited paired samples. However, their performance currently falls short of the state-of-the-art fully supervised methods.

Building upon the success of the diffusion model in various low-level visual tasks [Kawar *et al.*, 2022; Fei *et al.*, 2023], we approach UIE as a conditional generation problem. Our objective is to model and sample the posterior probability density of the enhanced image given an underwater image. To achieve this, we propose UIEDP, a novel framework outlined in Figure 1 (c). Initially, we employ a diffusion model pre-trained on ImageNet [Deng *et al.*, 2009] as our generative model, which can capture the prior probability distribution of natural images. The denoising process of the diffusion model naturally generates realistic images. Subsequently, we utilize the output of any UIE algorithm as a pseudo-label image to guide the conditional generation, and sample from the posterior probability distribution of the enhanced image. If the UIE algorithm of generating pseudo labels is trained on synthetic paired datasets, the introduced diffusion prior can effectively counteract the adverse impact of unreal synthetic images. Furthermore, if the UIE algorithm does not require synthetic paired datasets training, the corresponding UIEDP is considered unsupervised. Experiments demonstrate that benefiting from the diffusion prior, the generated images consistently outperform both pseudo-label images and those produced by other UIE methods across various quality metrics.

In summary, our main contributions are twofold: (1) We design UIEDP, a novel diffusion-based framework for UIE from the perspective of conditional generation. UIEDP can make full use of the generative prior of the pre-trained diffusion model to generate higher-quality enhanced images. Notably, UIEDP is adaptable to both supervised and unsupervised settings, showcasing its versatility. (2) Extensive experiments and ablation studies demonstrate the effectiveness of our framework and illustrate the impact of each component.

2 Related Work

Underwater Image Enhancement. Existing UIE methods can be divided into three categories: physical model-based, physical model-free, and data-driven methods. Physical model-based methods estimate the parameters of the underwater image formation model to invert the degradation process. For example, UDCP [Drews *et al.*, 2013] proposes a variant of DCP [He *et al.*, 2010] that estimates the transmission map through the blue and green color channels, while Galdran *et al.* [2015] proposed a red channel method to recover colors associated to short wavelengths. Sea-thru [Akkaynak and Treibitz, 2019] replaces the atmospheric image formation model with a physically accurate model and restores color based on RGBD images. However, these methods are sensitive to the assumptions made in estimating the model parameters and thus have few applicable scenes and poor robustness. To improve the visual quality, physical model-free methods directly adjust image pixel values by histogram equalization [Hitam *et al.*, 2013], color balance [Zhang *et al.*, 2022; Ancuti *et al.*, 2017], and contrast correlation [Ghani and Isa, 2015]. Fusion [Ancuti *et al.*, 2012] is one typical method of these, which pro-

duces a more pleasing image by blending color-corrected and contrast-enhanced versions of the original underwater image. However, these methods often suffer from over-enhancement, color distortions, and artifacts when encountered with sophisticated illumination conditions [Zhuang *et al.*, 2022].

Recently, many works have focused on using deep learning techniques in UIE. However, obtaining reference images for underwater scenes is challenging, leading researchers to employ various methods to synthesize paired datasets. Li *et al.* [2020] synthesized paired data based on underwater scene priors. Additionally, several GAN-based methods [Fabbri *et al.*, 2018; Islam *et al.*, 2020] have been trained adversarially by the generated paired datasets. Li *et al.* [2019a] constructed a paired dataset UIEB by using the best result of several enhancement algorithms to obtain a reference image. Peng *et al.* [2023] collected a larger dataset LSUI and used it to train a Transformer-based model. These paired datasets have facilitated the development of many UIE models. Some models have incorporated physical priors, such as multi-color space inputs [Li *et al.*, 2021; Wang *et al.*, 2021] and depth maps [Cong *et al.*, 2023], to generate visually appealing images. To enhance the efficiency of UIE, Jiang *et al.* [2023] proposed a highly efficient and lightweight real-time UIE network with only 9k parameters. In addition to these fully supervised methods, there are also unsupervised [Fu *et al.*, 2022] and semi-supervised [Huang *et al.*, 2023] methods.

Diffusion Models. Denoising diffusion probabilistic model (DDPM) [Ho *et al.*, 2020] is a new generative framework that is utilized to model complex data distributions and generate high-quality images. Based on DDPM, the denoising diffusion implicit model (DDIM) [Song *et al.*, 2020] introduces a class of non-Markovian diffusion processes to accelerate the sampling process. In order to achieve conditional generation, Dhariwal *et al.* [2021] have conditioned the pre-trained diffusion model during sampling with the gradients of a classifier. An alternative way is to explicitly introduce the conditional information as input to the diffusion models [Saharia *et al.*, 2022]. Benefiting from conditional generation, the diffusion models have also been successfully applied to various image restoration tasks [Fei *et al.*, 2023], including denoising, deblurring, and inpainting [Zhu *et al.*, 2023; Lugmayr *et al.*, 2022; Kawar *et al.*, 2022]. However, to our best knowledge, only Tang *et al.* [2023] have applied a lightweight diffusion model to underwater image enhancement in a supervised manner. In contrast, our approach does not train the diffusion model from scratch but rather makes full use of the natural image priors that are inherent in the pre-trained diffusion model. Furthermore, our method is also applicable to unsupervised scenarios.

3 Methodology

3.1 Preliminary of Diffusion Models

Denoising diffusion probabilistic model [Sohl-Dickstein *et al.*, 2015; Ho *et al.*, 2020] is a type of generative model that converts the isotropic Gaussian distribution into a data distribution. It mainly consists of the diffusion process and the reverse process. The diffusion process is a Markov chain that

gradually adds noise to data x_0 at T time steps. Each step of the diffusion process can be written as:

$$q(x_t|x_{t-1}) = \mathcal{N}(x_t; \sqrt{1 - \beta_t}x_{t-1}, \beta_t\mathbf{I}), \quad (1)$$

where β_1, \dots, β_T is a fixed variance schedule. Using the notation $\alpha_t = 1 - \beta_t$ and $\bar{\alpha}_t = \prod_{s=1}^t \alpha_s$, we can sample x_t at an arbitrary timestep according to a closed form:

$$x_t = \sqrt{\bar{\alpha}_t}x_0 + \sqrt{1 - \bar{\alpha}_t}\epsilon, \quad (2)$$

where ϵ is Gaussian noise.

To recover the data from the noise, each step of the reverse process can be defined as:

$$p_\theta(x_{t-1}|x_t) = \mathcal{N}(x_{t-1}; \mu_\theta(x_t, t), \Sigma_\theta\mathbf{I}), \quad (3)$$

where $\mu_\theta(x_t, t)$ is the mean, and variance Σ_θ can be set as learnable parameters [Nichol and Dhariwal, 2021] or constants [Ho *et al.*, 2020]. By using reparameterization techniques, the mean can be transformed into:

$$\mu_\theta(x_t, t) = \frac{1}{\sqrt{\alpha_t}} \left(x_t - \frac{\beta_t}{\sqrt{1 - \bar{\alpha}_t}} \epsilon_\theta(x_t, t) \right), \quad (4)$$

where ϵ_θ is a function approximator intended to predict the noise ϵ in Equation 2 from x_t . By substituting the predicted noise $\epsilon_\theta(x_t, t)$ into Equation 2, we can predict the data \tilde{x}_0 from x_t :

$$\tilde{x}_0 = \frac{1}{\sqrt{\alpha_t}}x_t - \frac{\sqrt{1 - \bar{\alpha}_t}}{\sqrt{\alpha_t}}\epsilon_\theta(x_t, t). \quad (5)$$

To perform conditional generation, Dhariwal *et al.* [2021] introduced a classifier $p_\phi(y|x_t)$, and each step of the reverse process conditioned on y can be rewritten as:

$$\begin{aligned} \log p_\theta(x_{t-1}|x_t, y) &= \log(p_\theta(x_{t-1}|x_t)p_\phi(y|x_t)) + C_1 \\ &\approx \log p(z) + C_2, \end{aligned} \quad (6)$$

where $z \sim \mathcal{N}(\mu + \Sigma g, \Sigma)$, μ and Σ are the mean and variance of the distribution $p_\theta(x_{t-1}|x_t)$ respectively. C_1 and C_2 are constants. g is the gradient of the classifier:

$$g = \nabla_{x_t} \log p_\phi(y|x_t)|_{x_t=\mu}. \quad (7)$$

Therefore, the conditional transition operator can be approximated by shifting the mean at each time step by Σg .

3.2 Proposed UIEDP

Given an underwater image y , the objective of UIE is to generate the enhanced image x_0 by searching within the domain of natural images \mathcal{D} to discover a natural image x_0 that best matches y . Therefore, UIE can be conceptualized as sampling from the posterior probability, $p(x_0|y)$, conditioned on y . Due to the stronger generative capabilities demonstrated by diffusion models over other generative models, we utilize a DDPM pre-trained on ImageNet [Deng *et al.*, 2009] to establish the prior probability, $p(x_0)$, within the natural image domain. Following Dhariwal *et al.* [2021] and Equation 6, we can formulate each step in the reverse process (conditional sampling) as:

$$p_\theta(x_{t-1}|x_t, y) = C_3 p_\theta(x_{t-1}|x_t) p(y|x_t), \quad (8)$$

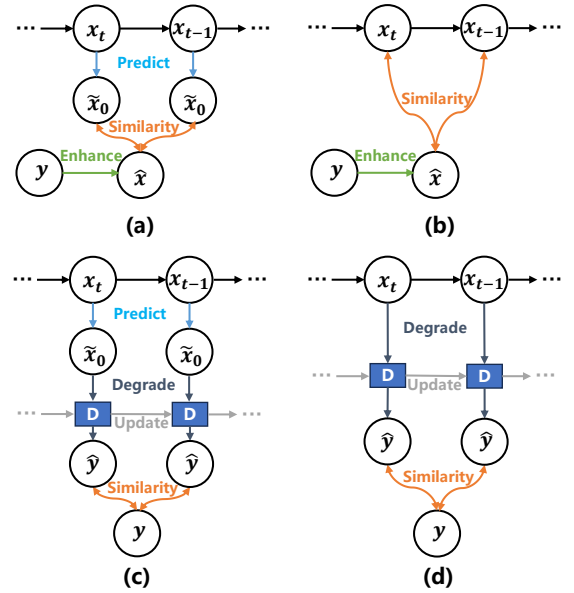


Figure 2: Four different guidance methods: guidance on (a) \tilde{x}_0 and natural image domain, (b) x_t and natural image domain, (c) \tilde{x}_0 and underwater image domain, (d) x_t and underwater image domain. The blue block D represents the underwater imaging model.

where C_3 is a constant. The former item $p_\theta(x_{t-1}|x_t)$ can be derived from the pre-trained diffusion model, capturing the transition probability from x_t to x_{t-1} . $p_\theta(x_{t-1}|x_t)$ is a Gaussian distribution, and we use μ and Σ to denote its mean and variance. Meanwhile, the latter item $p(y|x_t)$ represents the guided item, which can be modeled by a classifier when y corresponds to a specific category. However, in the context of UIE, the role of $p(y|x_t)$ differs. Instead of categorization, we expect $p(y|x_t)$ to quantify the degree of matching between the observed underwater image y and the sampled image x_t . Following Avrahami *et al.* [2022], we directly model the negative logarithm of $p(y|x_t)$ using a matching function $\mathcal{L}_{match}(y, x_t)$:

$$-\log p(y|x_t) = \mathcal{L}_{match}(y, x_t), \quad (9)$$

where the specific implementation of $\mathcal{L}_{match}(y, x_t)$ is left to the following text. Substituting $\mathcal{L}_{match}(y, x_t)$ into Equation 7, the new gradient of $p(y|x_t)$ is:

$$g = -\nabla_x \mathcal{L}_{match}(y, x_t)|_{x_t=\mu}. \quad (10)$$

Therefore, we can shift the mean μ by Σg during sampling to guide the generation. Next, we explore the design of the matching function $\mathcal{L}_{match}(y, x_t)$, which determines the way guidance is applied.

Guidance on x_t or \tilde{x}_0 . At each sampling step, in addition to the image x_t sampled from the diffusion model, we also have \tilde{x}_0 which can be predicted from x_t . According to Equation 5, \tilde{x}_0 is known when x_t is given. Therefore, $p(y|x_t) = p(y|\tilde{x}_0)$. Similarly, we can use the matching function $\mathcal{L}_{match}(y, \tilde{x}_0)$ to model the negative logarithm of $p(y|\tilde{x}_0)$, and the gradient g can be calculated by $g =$

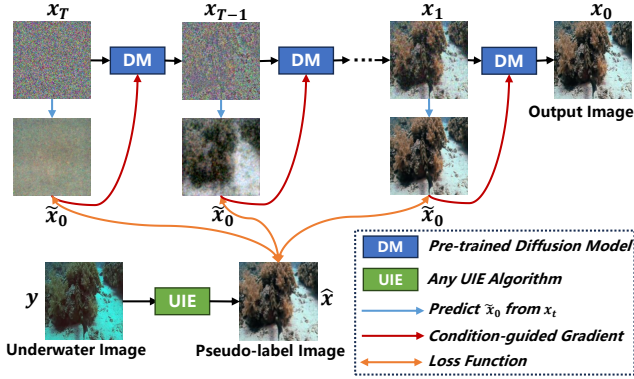


Figure 3: The overall framework of UIEDP. Guided by pseudo-labeled images generated from underwater imagery, a pre-trained diffusion model progressively denoises Gaussian noise images, yielding the corresponding enhanced images.

$-\nabla_{\tilde{x}_0} \mathcal{L}_{match}(y, \tilde{x}_0)$. Therefore, we have two different guidance methods: guidance on x_t (Figure 2 (b) (d)) and guidance on \tilde{x}_0 (Figure 2 (a) (c)).

Whether the guidance is on x_t ($x = x_t$) or \tilde{x}_0 ($x = \tilde{x}_0$), x belongs to the natural image domain, whereas y belongs to the underwater image domain. Hence, we need to transform x and y into the same domain before measuring the degree of matching $\mathcal{L}_{match}(y, x)$. Similar to Figure 1, there are two implementation approaches.

Guidance on Natural Image Domain. We can transform y into the natural image domain to align with x . As shown in Figure 2 (a) (b), we use any other UIE algorithm to enhance y to generate the pseudo-label image \hat{x} . Then, we calculate the similarity $\mathcal{L}_{sim}(\hat{x}, x)$ between the generated image and the pseudo-label image as the matching function $\mathcal{L}_{match}(y, x)$. It is worth noting that if the UIE algorithm used to generate the pseudo-label image \hat{x} does not require supervised training, the corresponding UIEDP is also considered unsupervised.

Guidance on Underwater Image Domain. We can also transform x into the underwater image domain. Referring to the modified Koschmieder’s light scattering model [Fu *et al.*, 2022], the degradation of underwater images can be formulated as:

$$\hat{y} = x * T + (1 - T) * A, \quad (11)$$

where A is the global background light and T is the medium transmission map representing the percentage of scene radiance reaching the camera after underwater reflection. For each underwater image, we estimate its A by Gaussian blur [Fu *et al.*, 2022] and T by GDCP [Peng *et al.*, 2018]. However, the estimated transmission map may be inaccurate, resulting in an unrealistic underwater image \hat{y} . Inspired by Fei *et al.* [2023], we continually update T by gradient descent at each sampling step. After obtaining \hat{y} , we calculate the similarity $\mathcal{L}_{sim}(y, \hat{y})$ between the real underwater image and the synthesized version as the matching function $\mathcal{L}_{match}(y, x)$, as shown in Figure 2 (c) (d). As no additional UIE algorithm is required, UIEDP which applies guidance on the underwater image domain is unsupervised.

Algorithm 1 UIEDP algorithm

Input: Underwater image y , any other UIE algorithm $\text{Enhance}(\cdot)$, pre-trained diffusion model $(\mu_\theta(x_t), \Sigma_\theta(x_t), \epsilon_\theta(x_t, t))$, loss function \mathcal{L} , and gradient scale s

Output: Enhanced image x_0

- 1: $\hat{x} \leftarrow \text{Enhance}(y)$
- 2: Sample $x_T \sim \mathcal{N}(0, \mathbf{I})$
- 3: **for** $t = T, \dots, 1$ **do**
- 4: $\mu, \Sigma \leftarrow \mu_\theta(x_t), \Sigma_\theta(x_t)$
- 5: $\tilde{x}_0 \leftarrow \frac{1}{\sqrt{\alpha_t}} x_t - \frac{\sqrt{1-\alpha_t}}{\sqrt{\alpha_t}} \epsilon_\theta(x_t, t)$
- 6: $g \leftarrow -\nabla_{\tilde{x}_0} \mathcal{L}(\hat{x}, \tilde{x}_0)$
- 7: Sample $x_{t-1} \sim \mathcal{N}(\mu + sg, \Sigma)$
- 8: **end for**
- 9: **return** x_0

By selecting the variables (x_t or \tilde{x}_0) and domains (natural or underwater) of the guidance, we have four different ways to implement the matching function $\mathcal{L}_{match}(y, x)$, as shown in Figure 2. We have conducted a comprehensive comparison and found that applying guidance on \tilde{x}_0 and natural image domain (Figure 2 (a)) is the best choice, as detailed in Section 4.4. Therefore, we implement UIEDP based on this guidance method.

As shown in Figure 3, we first utilize any other UIE algorithm to transform the underwater image y into the natural image domain, getting the pseudo-label image \hat{x} . Then we predict the mean μ and \tilde{x}_0 from the sampled image x_t at each sampling step. To improve the quality of the enhanced image, we add the image quality function of \tilde{x}_0 to the similarity function $\mathcal{L}_{sim}(\hat{x}, \tilde{x}_0)$ between \hat{x} and \tilde{x}_0 , obtaining the overall loss function $\mathcal{L}(\hat{x}, \tilde{x}_0)$. The gradient of the loss function $g = -\nabla_{\tilde{x}_0} \mathcal{L}(\hat{x}, \tilde{x}_0)$ is used to guide the conditional generation. Besides, we find that the variance Σ negatively influences the generated image [Fei *et al.*, 2023]. Therefore, we shift the mean μ by sg instead of $s\Sigma g$, where s is the gradient scale. Algorithm 1 summarizes the steps of our UIEDP algorithm, and algorithms about other three guidance methods (Figure 2 (b) (c) (d)) can be found in the appendix.

3.3 Loss Function

The loss function $\mathcal{L}(\hat{x}, \tilde{x}_0)$ is a key factor in guiding conditional generation, mainly composed of two parts: the similarity $\mathcal{L}_{sim}(\hat{x}, \tilde{x}_0)$ between \hat{x} and \tilde{x}_0 , and the quality of \tilde{x}_0 .

Similarity between \hat{x} and \tilde{x}_0 . In addition to the MAE loss $\mathcal{L}_{MAE}(\hat{x}, \tilde{x}_0)$, the similarity measure also incorporates the multiscale SSIM loss $\mathcal{L}_{MSSIM}(\hat{x}, \tilde{x}_0)$ [Wang *et al.*, 2003] and the perceptual loss $\mathcal{L}_{Perceptual}(\hat{x}, \tilde{x}_0)$ [Johnson *et al.*, 2016]. The multiscale SSIM loss mimics the human visual system to measure the multi-scale structural similarity of two images, while the perceptual loss measures the semantic content similarity at the feature level.

Quality of \tilde{x}_0 . URanker [Guo *et al.*, 2023] is a transformer trained on an underwater image quality ranking dataset, capable of producing quality scores for underwater images. MUSIQ [Ke *et al.*, 2021] is a popular Transformer-based natural image quality assessment (IQA) that has been proven to perform better than other traditional IQA metrics [Huang *et*

Methods	T90					C60					U45				
	PSNR \uparrow	SSIM \uparrow	UCIQE \uparrow	UIQM \uparrow	NIQE \downarrow	URanker \uparrow	MUSIQ \uparrow	UCIQE \uparrow	UIQM \uparrow	NIQE \downarrow	URanker \uparrow	MUSIQ \uparrow	UCIQE \uparrow	UIQM \uparrow	NIQE \downarrow
GDCP	13.89	0.75	0.60	2.54	4.93	0.45	46.19	0.57	2.25	6.27	0.54	47.95	0.59	2.25	4.14
Fusion	23.14	0.89	0.63	2.86	4.98	1.43	44.74	0.61	2.61	5.91	1.68	47.62	0.64	2.97	8.02
UWCNN	19.02	0.82	0.55	2.79	4.72	0.56	42.13	0.51	2.52	5.94	0.36	46.96	0.48	3.04	4.09
UGAN	17.42	0.76	0.58	<u>3.10</u>	5.81	0.68	41.12	0.55	2.86	6.90	0.89	43.96	0.57	3.10	5.79
FUnLEGAN	16.97	0.73	0.57	3.06	4.92	0.42	41.55	0.55	2.87	6.06	0.80	45.68	0.56	2.92	4.45
MLLE	19.48	0.84	0.60	2.45	4.87	<u>1.89</u>	<u>47.97</u>	0.57	2.21	5.85	<u>2.68</u>	<u>51.67</u>	0.59	2.48	4.83
UShape	20.24	0.81	0.59	3.06	<u>4.67</u>	1.11	37.67	0.56	2.73	5.60	1.57	41.10	0.57	3.19	4.20
Ucolor	20.86	0.88	0.58	3.01	4.75	0.92	45.33	0.55	2.62	6.14	1.60	47.28	0.58	3.20	4.71
UIEC ² Net	<u>23.26</u>	0.91	0.62	3.06	4.71	1.58	43.07	0.59	2.78	<u>5.39</u>	1.93	48.82	0.61	<u>3.26</u>	<u>3.91</u>
NU ² Net	22.93	0.90	0.61	2.98	4.81	1.55	42.32	0.58	2.63	5.64	1.86	48.90	0.59	3.23	4.06
FA ⁺ Net	20.98	0.88	0.59	2.92	4.83	1.26	42.41	0.57	2.52	5.70	1.59	47.50	0.58	3.21	4.02
UIEDP	23.44	0.91	0.63	3.13	4.54	2.16	51.63	<u>0.59</u>	2.87	5.21	3.58	57.17	<u>0.61</u>	3.27	3.79

Table 1: Comparison with the state-of-the-art results on T90, C60, and U45. **Bold** and underlined denote the best and second-best results in each column, respectively. \uparrow represents the higher is the better as well as \downarrow represents the lower is the better.

al., 2023]. Therefore, we introduce these two differentiable losses: $\mathcal{L}_{URanker}(\hat{x}_0)$ and $\mathcal{L}_{MUSIQ}(\hat{x}_0)$.

The overall loss function $\mathcal{L}(\hat{x}, \tilde{x}_0)$ during sampling is a weighted sum of the above five losses:

$$\begin{aligned} \mathcal{L}(\hat{x}, \tilde{x}_0) = & \mathcal{L}_{MAE}(\hat{x}, \tilde{x}_0) - \lambda_1 \mathcal{L}_{MSSSIM}(\hat{x}, \tilde{x}_0) \\ & + \lambda_2 \mathcal{L}_{Perceptual}(\hat{x}, \tilde{x}_0) - \lambda_3 \mathcal{L}_{URanker}(\hat{x}_0) \\ & - \lambda_4 \mathcal{L}_{MUSIQ}(\hat{x}_0), \end{aligned} \quad (12)$$

where λ_1 , λ_2 , λ_3 and λ_4 are hyper-parameters to balance the contribution of each loss.

4 Experiments

4.1 Datasets and Evaluation Metrics

We empirically evaluate the performance of UIEDP on two public datasets: UIEB [Li *et al.*, 2019a] and U45 [Li *et al.*, 2019b]. The UIEB dataset consists of 890 raw underwater images and corresponding high-quality reference images. Following FA⁺Net [Jiang *et al.*, 2023], we use 800 pairs of these images as the training set, and the remaining 90 pairs of images as the test set, named **T90**. In addition, the UIEB dataset also includes a set of 60 challenge images (**C60**) that do not have corresponding reference images. The **U45** dataset contains 45 carefully selected underwater images, serving as an important benchmark for UIE. For all the supervised methods, we train the models on the training set of UIEB and test them on the T90, C60, and U45 datasets.

In the above three test sets, each underwater image in T90 is paired with a corresponding reference image, while C60 and U45 only contain underwater images. Therefore, we evaluate the performance of UIE using two full-reference image quality evaluation metrics and five non-reference image quality assessment (NR-IQA) metrics. PSNR and SSIM are commonly used full-reference metrics for evaluating generation tasks, measuring the similarity between the enhanced images and the reference images. For non-reference metrics, we have adopted three metrics specifically designed for UIE tasks: UIQM [Panetta *et al.*, 2015], UCIQE [Yang and Sowmya, 2015], and URanker [Guo *et al.*, 2023], along with two natural image quality assessment metrics: NIQE [Mittal *et al.*, 2012] and MUSIQ [Ke *et al.*, 2021]. UIQM considers contrast, sharpness, and colorfulness of the image, while



Figure 4: Comparison between the pseudo-labeled images and the images generated by UIEDP. The last column denotes their difference images.

UCIQE considers brightness instead of sharpness. NIQE analyzes the statistical properties of the image to measure the level of noise and distortion.

4.2 Implementation Details

We replicated all the compared methods based on their official codes and hyperparameters. For models requiring supervised training, we trained them for 100 epochs with a batch size of 32, using the ADAM optimizer [Kingma and Ba, 2014] with a learning rate 0.001. Data augmentation techniques such as horizontal flipping and rotation were employed during training. To ensure a fair comparison, all images were resized to 256×256 during both training and testing. Our UIEDP loaded weights of the unconditional diffusion model pre-trained on the ImageNet dataset (at a resolution of 256×256) provided by Dhariwal *et al.* [2021]. In all experiments, the weights $\lambda_1 = 1$, $\lambda_2 = 0.005$, $\lambda_4 = 0.00001$ in Equation 12. The gradient scale s is set to 12000 on T90 and 4000 on the other two datasets. λ_3 is set to 0.002 on U45 and 0.001 on the other two datasets.

4.3 Comparison with the State-of-the-art

We compare our method UIEDP with several state-of-the-art approaches, including one physical model-based method (GDCP [Peng *et al.*, 2018]), two physical model-free methods

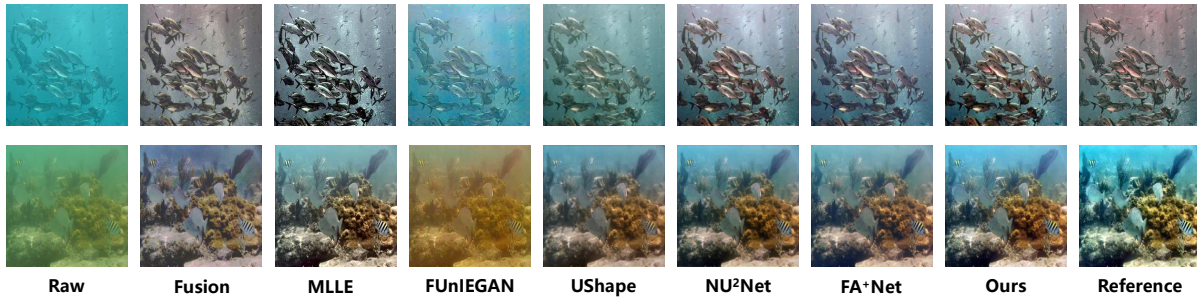


Figure 5: Visual comparison of different UIE methods on T90.

Method	URanker \uparrow	MUSIQ \uparrow	UCIQE \uparrow	UIQM \uparrow	NIQE \downarrow
USUIR	1.20	42.85	0.57	2.65	5.89
Fusion	1.43	44.74	0.61	2.61	5.91
UIEDP (Fusion)	2.14	52.69	0.61	2.75	5.80

Table 2: Comparison with two unsupervised methods on C60.

(Fusion [Ancuti *et al.*, 2012], MLE [Zhang *et al.*, 2022]), and eight data-driven methods (UWCNN [Li *et al.*, 2020], UGAN [Fabbri *et al.*, 2018], FUnIEGAN [Islam *et al.*, 2020], UShape [Peng *et al.*, 2023], UIEC²Net [Wang *et al.*, 2021], NU²Net [Guo *et al.*, 2023], FA⁺Net [Jiang *et al.*, 2023]). For our UIEDP, we employ UIEC²Net trained on the training set to generate pseudo-labeled images.

Results for three datasets are presented in Table 1. Experimental results demonstrate that compared to other methods, we achieve improvements in nearly all metrics across three datasets, particularly in NR-IQA metrics. It’s noteworthy that despite employing pseudo-labeled images generated by UIEC²Net for guiding conditional generation, UIEDP outperforms UIEC²Net across all metrics. This phenomenon can be attributed to UIEDP effectively harnessing the natural image priors inherent in the pre-trained diffusion model. Equation 8 indicates that conditional generation is jointly determined by priors and conditional guidance, thereby the introduction of diffusion prior enhances generation quality. Figure 4 visually illustrates the difference between output images of UIEDP and pseudo-labeled images. In the first example, the difference lies in the background lighting, with the image generated by UIEDP appearing brighter. In the second example, the difference lies in the jellyfish, where the image generated by UIEDP exhibits enhanced visual appeal.

Additionally, we present an intuitive comparison with other UIE methods in terms of visual effects. As shown in Figure 5, Fusion slightly distorts image colors and blurs image details; FUnIEGAN exhibits severe color distortion; MLE renders images overly sharp, presenting a black-and-white tone; UShape generates images with slightly dimmed background light; NU²Net and FA⁺Net fail to accommodate all underwater scenarios. For example, FA⁺Net performs well on the first example but poorly on the second. In contrast, the images generated by our UIEDP even appear better than the reference images, correcting the biased red or blue background light. This is attributed to the diffusion prior that is introduced by UIEDP. More visual comparisons are available

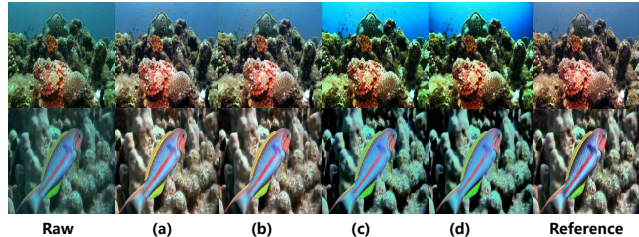


Figure 6: Visual comparison of four different guidance methods in Figure 2 on T90.

Guidance Method	PSNR \uparrow	SSIM \uparrow	UCIQE \uparrow	UIQM \uparrow	NIQE \downarrow	URanker \uparrow	MUSIQ \uparrow
Fig 2 (a) (Ours)	23.44	0.91	0.62	3.13	4.58	2.25	47.63
Fig 2 (b)	23.06	0.89	0.62	3.10	4.94	2.29	46.33
Fig 2 (c)	17.50	0.76	0.63	2.55	4.79	1.76	45.58
Fig 2 (d)	16.93	0.73	0.63	2.51	5.53	1.83	43.18

Table 3: Comparison of different guidance methods in Fig 2 on T90.

in the appendix.

Fusion [Ancuti *et al.*, 2012] enhances underwater images by adjusting color and contrast without the need for supervised training. Therefore, if we employ Fusion to generate pseudo-labeled images in UIEDP, UIEDP (Fusion) is considered unsupervised. We compare UIEDP with Fusion and another deep learning-based unsupervised method, USUIR [Fu *et al.*, 2022], and the experimental results are presented in Table 2. We observe that even USUIR falls short compared to Fusion, indicating the considerable challenge of UIE in an unsupervised setting. Moreover, the performance of UIEDP surpasses both of the two other methods.

4.4 Ablation Study

Ablations about guidance methods. In Figure 2, we propose four different guidance methods. Guidance can act on various variables (x_t or \tilde{x}_0) and image domains (natural or underwater). To find the optimal guidance method, we conduct both quantitative and qualitative analyses. For fair comparison, we omit quality assessment losses \mathcal{L}_{MUSIQ} and $\mathcal{L}_{URanker}$ in this ablation experiment. As shown in the last two rows of Table 3 and in Figure 6 (c) (d), guidance in the underwater image domain fails. This is because the degradation model in Equation 11 is a simplified imaging model that cannot precisely model real underwater imaging. And esti-

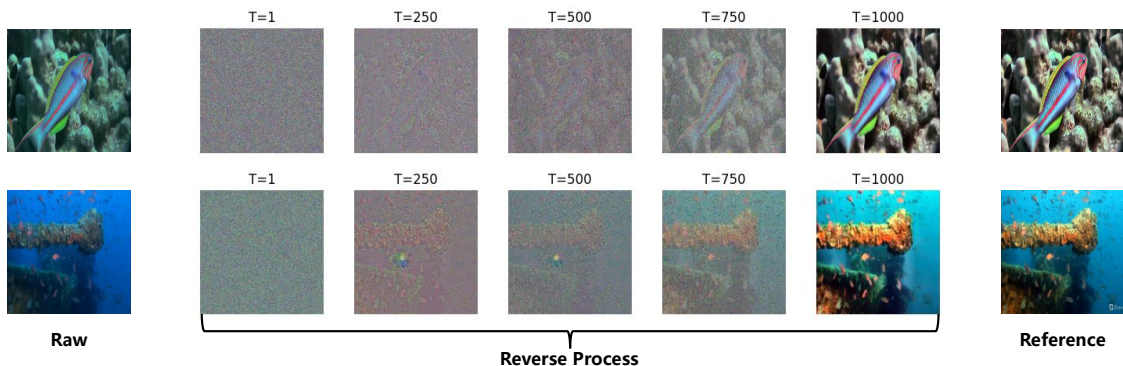


Figure 7: Visualization of the inverse diffusion process of UIEDP. The output images at 1000 steps are the final enhanced images.

mated global illumination and transmission maps may also be inaccurate. From Figure 6 (c) (d), the background light of the enhanced images is not normal. Although Figure 6 (a) and (b) looks visually similar, results in the first two rows of Table 3 suggest that guidance on \tilde{x}_0 yields better results than guidance on x_t . This is because in the early sampling steps, while x_t still appears as a noisy image, \tilde{x}_0 already resembles the outline of a normal image, as illustrated in Figure 3. From the above analysis, we find that applying guidance on \tilde{x}_0 and natural image domain (Figure 2 (a)) is the optimal guidance method.

Impact of the loss function. The loss function $\mathcal{L}(\hat{x}, \tilde{x}_0)$ plays a critical role in the sampling process, guiding conditional generation through its gradients. In UIEDP, we utilize a weighted sum of five losses as the total loss function $\mathcal{L}(\hat{x}, \tilde{x}_0)$. To investigate their contributions, we progressively introduce four additional losses alongside the MAE loss \mathcal{L}_{MAE} for experimental analysis. The comprehensive experimental results are detailed in Table 4. Notably, the inclusion of multiscale SSIM loss \mathcal{L}_{MSSSIM} and perceptual loss $\mathcal{L}_{Perceptual}$ both positively impact the generation process. These losses holistically gauge the similarity between generated images \tilde{x}_0 and pseudo-labeled images \hat{x} from various perspectives, leading to enhanced generation quality. Furthermore, MUSIQ \mathcal{L}_{MUSIQ} and URanker $\mathcal{L}_{URanker}$ losses significantly elevate the non-reference quality assessment for the generated images. Additionally, despite conditional generation being guided by pseudo-labeled images, UIEDP can produce higher-quality images compared to the provided pseudo-labeled images. This highlights that the pre-trained diffusion model on ImageNet inherently yields high-quality image outputs, which helps enhance low-quality underwater images.

Effect of sampling strategies and steps. DDIM [Song *et al.*, 2020] improves the sampling process over DDPM, allowing the generation of images of comparable quality with fewer steps. To explore the effect of sampling strategies, we replace the sampling process of UIEDP with DDIM. Experimental results in Table 5 indicate that images sampled via DDIM demonstrate inferior quality compared to DDPM. Additionally, in an effort to expedite generation speed, we attempt to directly reduce sampling steps. For DDIM, appropriately reducing the sampling steps yields better results. How-

Loss Function	PSNR \uparrow	SSIM \uparrow	UCIQE \uparrow	UIQM \uparrow	NIQE \downarrow	URanker \uparrow	MUSIQ \uparrow
Pseudo-label	23.26	0.91	0.62	3.06	4.71	2.20	47.71
\mathcal{L}_{MAE}	23.40	0.91	0.62	3.10	4.77	2.27	47.56
$+\mathcal{L}_{MSSSIM}$	23.42	0.91	0.62	3.10	4.72	2.27	47.55
$+\mathcal{L}_{Perceptual}$	23.44	0.91	0.62	3.13	4.58	2.25	47.63
$+\mathcal{L}_{URanker}$	23.43	0.91	0.62	3.12	4.60	2.44	47.77
$+\mathcal{L}_{MUSIQ}$	23.44	0.91	0.63	3.13	4.54	2.43	50.98

Table 4: Impact of the loss function $\mathcal{L}(\hat{x}, \tilde{x}_0)$ on T90. The first row indicates the quality of pseudo-labeled images, and the other rows indicate the quality of enhanced images generated by UIEDP under the guidance of different loss functions.

Method	Total steps	PSNR \uparrow	SSIM \uparrow	UCIQE \uparrow	UIQM \uparrow	NIQE \downarrow
DDIM	25	21.63	0.85	0.63	2.93	5.65
	50	20.08	0.79	0.64	2.94	5.66
DDPM	50	18.50	0.66	0.61	3.06	4.95
	250	22.40	0.88	0.62	3.12	4.69
	1000 (Ours)	23.44	0.91	0.63	3.13	4.54

Table 5: Effect of sampling strategies and steps on T90.

ever, reducing the sampling steps for DDPM leads to a decrease in the quality of generated images. In Figure 7, we visualize the images sampled from the intermediate steps when the total number of steps is 1000. Exploring how to enhance sampling efficiency is left for future research.

5 Conclusion

We propose a novel framework UIEDP for underwater image enhancement, which combines the pre-train diffusion model and any UIE algorithm to conduct conditional generation. The pre-trained diffusion model introduces the natural image prior, ensuring the capability to generate high-quality images. Simultaneously, any UIE algorithm provides pseudo-label images to guide conditional sampling, facilitating the generation of enhanced versions corresponding to underwater images. Additionally, UIEDP can work in either a supervised or unsupervised manner, depending on whether the UIE algorithm generating pseudo-labeled images requires paired samples for training. Extensive experiments show that UIEDP not only generates enhanced images of superior quality beyond the pseudo-labeled images but also surpasses other advanced UIE methods.

References

- [Akkaynak and Treibitz, 2019] Derya Akkaynak and Tali Treibitz. Sea-thru: A method for removing water from underwater images. In *Proceedings of the IEEE/CVF conference on computer vision and pattern recognition*, pages 1682–1691, 2019.
- [Ancuti *et al.*, 2012] Cosmin Ancuti, Codruta Orniana Ancuti, Tom Haber, and Philippe Bekaert. Enhancing underwater images and videos by fusion. In *2012 IEEE conference on computer vision and pattern recognition*, pages 81–88. IEEE, 2012.
- [Ancuti *et al.*, 2017] Codruta O Ancuti, Cosmin Ancuti, Christophe De Vleeschouwer, and Philippe Bekaert. Color balance and fusion for underwater image enhancement. *IEEE Transactions on image processing*, 27(1):379–393, 2017.
- [Avrahami *et al.*, 2022] Omri Avrahami, Dani Lischinski, and Ohad Fried. Blended diffusion for text-driven editing of natural images. In *Proceedings of the IEEE/CVF Conference on Computer Vision and Pattern Recognition (CVPR)*, pages 18208–18218, June 2022.
- [Chen and Pei, 2022] Yu-Wei Chen and Soo-Chang Pei. Domain adaptation for underwater image enhancement via content and style separation. *IEEE Access*, 10:90523–90534, 2022.
- [Cong *et al.*, 2023] Runmin Cong, Wenyu Yang, Wei Zhang, Chongyi Li, Chun-Le Guo, Qingming Huang, and Sam Kwong. Pugan: Physical model-guided underwater image enhancement using gan with dual-discriminators. *IEEE Transactions on Image Processing*, 2023.
- [Deng *et al.*, 2009] Jia Deng, Wei Dong, Richard Socher, Li-Jia Li, Kai Li, and Li Fei-Fei. Imagenet: A large-scale hierarchical image database. In *2009 IEEE conference on computer vision and pattern recognition*, pages 248–255. Ieee, 2009.
- [Dhariwal and Nichol, 2021] Prafulla Dhariwal and Alexander Nichol. Diffusion models beat gans on image synthesis. *Advances in neural information processing systems*, 34:8780–8794, 2021.
- [Drews *et al.*, 2013] Paul Drews, Erickson Nascimento, Filipe Moraes, Silvia Botelho, and Mario Campos. Transmission estimation in underwater single images. In *Proceedings of the IEEE international conference on computer vision workshops*, pages 825–830, 2013.
- [Fabbri *et al.*, 2018] Cameron Fabbri, Md Jahidul Islam, and Junaed Sattar. Enhancing underwater imagery using generative adversarial networks. In *2018 IEEE international conference on robotics and automation (ICRA)*, pages 7159–7165. IEEE, 2018.
- [Fei *et al.*, 2023] Ben Fei, Zhaoyang Lyu, Liang Pan, Junzhe Zhang, Weidong Yang, Tianyue Luo, Bo Zhang, and Bo Dai. Generative diffusion prior for unified image restoration and enhancement. In *Proceedings of the IEEE/CVF Conference on Computer Vision and Pattern Recognition*, pages 9935–9946, 2023.
- [Fu *et al.*, 2022] Zhenqi Fu, Huangxing Lin, Yan Yang, Shu Chai, Liyan Sun, Yue Huang, and Xinghao Ding. Unsupervised underwater image restoration: From a homology perspective. In *Proceedings of the AAAI Conference on Artificial Intelligence*, volume 36, pages 643–651, 2022.
- [Galdran *et al.*, 2015] Adrian Galdran, David Pardo, Artzai Picón, and Aitor Alvarez-Gila. Automatic red-channel underwater image restoration. *Journal of Visual Communication and Image Representation*, 26:132–145, 2015.
- [Ghani and Isa, 2015] Ahmad Shahrizan Abdul Ghani and Nor Ashidi Mat Isa. Enhancement of low quality underwater image through integrated global and local contrast correction. *Applied Soft Computing*, 37:332–344, 2015.
- [Guo *et al.*, 2023] Chunle Guo, Ruiqi Wu, Xin Jin, Linghao Han, Weidong Zhang, Zhi Chai, and Chongyi Li. Underwater ranker: Learn which is better and how to be better. In *Proceedings of the AAAI conference on artificial intelligence*, volume 37, pages 702–709, 2023.
- [He *et al.*, 2010] Kaiming He, Jian Sun, and Xiaoou Tang. Single image haze removal using dark channel prior. *IEEE transactions on pattern analysis and machine intelligence*, 33(12):2341–2353, 2010.
- [Hitam *et al.*, 2013] Muhammad Suzuri Hitam, Ezmahamrul Afreen Awalludin, Wan Nural Jawahir Hj Wan Yussof, and Zainuddin Bachok. Mixture contrast limited adaptive histogram equalization for underwater image enhancement. In *2013 International conference on computer applications technology (ICCAT)*, pages 1–5. IEEE, 2013.
- [Ho *et al.*, 2020] Jonathan Ho, Ajay Jain, and Pieter Abbeel. Denoising diffusion probabilistic models. *Advances in neural information processing systems*, 33:6840–6851, 2020.
- [Huang *et al.*, 2023] Shirui Huang, Keyan Wang, Huan Liu, Jun Chen, and Yunsong Li. Contrastive semi-supervised learning for underwater image restoration via reliable bank. In *Proceedings of the IEEE/CVF Conference on Computer Vision and Pattern Recognition*, pages 18145–18155, 2023.
- [Islam *et al.*, 2020] Md Jahidul Islam, Youya Xia, and Junaed Sattar. Fast underwater image enhancement for improved visual perception. *IEEE Robotics and Automation Letters*, 5(2):3227–3234, 2020.
- [Jiang *et al.*, 2023] Jingxia Jiang, Tian Ye, Jinbin Bai, Sixiang Chen, Wenhao Chai, Shi Jun, Yun Liu, and Erkang Chen. Five a+ network: You only need 9k parameters for underwater image enhancement. *arXiv preprint arXiv:2305.08824*, 2023.
- [Johnson *et al.*, 2016] Justin Johnson, Alexandre Alahi, and Li Fei-Fei. Perceptual losses for real-time style transfer and super-resolution. In *Computer Vision—ECCV 2016: 14th European Conference, Amsterdam, The Netherlands, October 11–14, 2016, Proceedings, Part II 14*, pages 694–711. Springer, 2016.
- [Kawar *et al.*, 2022] Bahjat Kawar, Michael Elad, Stefano Ermon, and Jiaming Song. Denoising diffusion restora-

- tion models. *Advances in Neural Information Processing Systems*, 35:23593–23606, 2022.
- [Ke *et al.*, 2021] Junjie Ke, Qifei Wang, Yilin Wang, Peyman Milanfar, and Feng Yang. Musiq: Multi-scale image quality transformer. In *Proceedings of the IEEE/CVF International Conference on Computer Vision*, pages 5148–5157, 2021.
- [Kingma and Ba, 2014] Diederik P Kingma and Jimmy Ba. Adam: A method for stochastic optimization. In *International Conference on Learning Representations*, 2014.
- [Li *et al.*, 2019a] Chongyi Li, Chunle Guo, Wenqi Ren, Runmin Cong, Junhui Hou, Sam Kwong, and Dacheng Tao. An underwater image enhancement benchmark dataset and beyond. *IEEE Transactions on Image Processing*, 29:4376–4389, 2019.
- [Li *et al.*, 2019b] Hanyu Li, Jingjing Li, and Wei Wang. A fusion adversarial underwater image enhancement network with a public test dataset. *arXiv preprint arXiv:1906.06819*, 2019.
- [Li *et al.*, 2020] Chongyi Li, Saeed Anwar, and Fatih Porikli. Underwater scene prior inspired deep underwater image and video enhancement. *Pattern Recognition*, 98:107038, 2020.
- [Li *et al.*, 2021] Chongyi Li, Saeed Anwar, Junhui Hou, Runmin Cong, Chunle Guo, and Wenqi Ren. Underwater image enhancement via medium transmission-guided multi-color space embedding. *IEEE Transactions on Image Processing*, 30:4985–5000, 2021.
- [Lugmayr *et al.*, 2022] Andreas Lugmayr, Martin Danelljan, Andres Romero, Fisher Yu, Radu Timofte, and Luc Van Gool. Repaint: Inpainting using denoising diffusion probabilistic models. In *Proceedings of the IEEE/CVF Conference on Computer Vision and Pattern Recognition*, pages 11461–11471, 2022.
- [Mittal *et al.*, 2012] Anish Mittal, Rajiv Soundararajan, and Alan C Bovik. Making a “completely blind” image quality analyzer. *IEEE Signal processing letters*, 20(3):209–212, 2012.
- [Nichol and Dhariwal, 2021] Alexander Quinn Nichol and Prafulla Dhariwal. Improved denoising diffusion probabilistic models. In *International Conference on Machine Learning*, pages 8162–8171. PMLR, 2021.
- [Panetta *et al.*, 2015] Karen Panetta, Chen Gao, and Sos Agaian. Human-visual-system-inspired underwater image quality measures. *IEEE Journal of Oceanic Engineering*, 41(3):541–551, 2015.
- [Peng *et al.*, 2018] Yan-Tsung Peng, Keming Cao, and Pamela C Cosman. Generalization of the dark channel prior for single image restoration. *IEEE Transactions on Image Processing*, 27(6):2856–2868, 2018.
- [Peng *et al.*, 2023] Lintao Peng, Chunli Zhu, and Liheng Bian. U-shape transformer for underwater image enhancement. *IEEE Transactions on Image Processing*, 2023.
- [Saharia *et al.*, 2022] Chitwan Saharia, Jonathan Ho, William Chan, Tim Salimans, David J Fleet, and Mohammad Norouzi. Image super-resolution via iterative refinement. *IEEE Transactions on Pattern Analysis and Machine Intelligence*, 45(4):4713–4726, 2022.
- [Sohl-Dickstein *et al.*, 2015] Jascha Sohl-Dickstein, Eric Weiss, Niru Maheswaranathan, and Surya Ganguli. Deep unsupervised learning using nonequilibrium thermodynamics. In *International conference on machine learning*, pages 2256–2265. PMLR, 2015.
- [Song *et al.*, 2020] Jiaming Song, Chenlin Meng, and Stefano Ermon. Denoising diffusion implicit models. *arXiv preprint arXiv:2010.02502*, 2020.
- [Tang *et al.*, 2023] Yi Tang, Hiroshi Kawasaki, and Takafumi Iwaguchi. Underwater image enhancement by transformer-based diffusion model with non-uniform sampling for skip strategy. In *Proceedings of the 31st ACM International Conference on Multimedia*, pages 5419–5427, 2023.
- [Wang *et al.*, 2003] Zhou Wang, Eero P Simoncelli, and Alan C Bovik. Multiscale structural similarity for image quality assessment. In *The Thirty-Seventh Asilomar Conference on Signals, Systems & Computers, 2003*, volume 2, pages 1398–1402. Ieee, 2003.
- [Wang *et al.*, 2019] Nan Wang, Yabin Zhou, Fenglei Han, Haitao Zhu, and Jingzheng Yao. Uwgan: underwater gan for real-world underwater color restoration and dehazing. *arXiv preprint arXiv:1912.10269*, 2019.
- [Wang *et al.*, 2021] Yudong Wang, Jichang Guo, Huan Gao, and Huihui Yue. Uiec2-net: Cnn-based underwater image enhancement using two color space. *Signal Processing: Image Communication*, 96:116250, 2021.
- [Wang *et al.*, 2023] Zhengyong Wang, Liquan Shen, Mai Xu, Mei Yu, Kun Wang, and Yufei Lin. Domain adaptation for underwater image enhancement. *IEEE Transactions on Image Processing*, 32:1442–1457, 2023.
- [Yang and Sowmya, 2015] Miao Yang and Arcot Sowmya. An underwater color image quality evaluation metric. *IEEE Transactions on Image Processing*, 24(12):6062–6071, 2015.
- [Zhang *et al.*, 2022] Weidong Zhang, Peixian Zhuang, Haihan Sun, Guohou Li, Sam Kwong, and Chongyi Li. Underwater image enhancement via minimal color loss and locally adaptive contrast enhancement. *IEEE Transactions on Image Processing*, 31:3997–4010, 2022.
- [Zhu *et al.*, 2023] Yuanzhi Zhu, Kai Zhang, Jingyun Liang, Jiezhong Cao, Bihan Wen, Radu Timofte, and Luc Van Gool. Denoising diffusion models for plug-and-play image restoration. In *Proceedings of the IEEE/CVF Conference on Computer Vision and Pattern Recognition*, pages 1219–1229, 2023.
- [Zhuang *et al.*, 2022] Peixian Zhuang, Jiamin Wu, Fatih Murat Porikli, and Chongyi Li. Underwater image enhancement with hyper-laplacian reflectance priors. *IEEE Transactions on Image Processing*, 31:5442–5455, 2022.

A Limitations and Future Work

Like other diffusion-based methods, the primary drawback of UIEDP is the requirement for many sampling steps, hindering its application in scenarios that demand real-time enhancement. Hence, future research will focus on enhancing the generation efficiency of UIEDP. In the realm of diffusion models, several works have tried to generate high-quality images with fewer sampling steps. Exploring the application of acceleration techniques employed in these studies to enhance the efficiency of UIEDP stands as a promising avenue for exploration.

B More Algorithms

In this section, we elaborate on the implementation of three other guidance methods mentioned in Figure 2 of the main paper, along with the integration of DDIM within UIEDP. Algorithms 2, 3, 4 correspond to the three guidance methods depicted in Figure 2 (b) (c) (d), respectively. Algorithm 5 delineates the steps involved in utilizing DDIM for sampling within UIEDP.

Algorithm 2 Guidance on x_t and natural image domain

Input: Underwater image y , any other UIE algorithm $\text{Enhance}(\cdot)$, pre-trained diffusion model $(\mu_\theta(x_t), \Sigma_\theta(x_t))$, loss function \mathcal{L} , and gradient scale s

Output: Enhanced image x_0

- 1: $\hat{x} \leftarrow \text{Enhance}(y)$
 - 2: Sample $x_T \sim \mathcal{N}(0, \mathbf{I})$
 - 3: **for** $t = T, \dots, 1$ **do**
 - 4: $\mu, \Sigma \leftarrow \mu_\theta(x_t), \Sigma_\theta(x_t)$
 - 5: $g \leftarrow -\nabla_{x_t} \mathcal{L}(\hat{x}, x_t)$
 - 6: Sample $x_{t-1} \sim \mathcal{N}(\mu + sg, \Sigma)$
 - 7: **end for**
 - 8: **return** x_0
-

Algorithm 3 Guidance on \tilde{x}_0 and underwater image domain

Input: Underwater image y , global background light A , transmission map T , learning rate l for optimizing T , pre-trained diffusion model $(\mu_\theta(x_t), \Sigma_\theta(x_t), \epsilon_\theta(x_t, t))$, loss function \mathcal{L} , and gradient scale s

Output: Enhanced image x_0

- 1: Sample $x_T \sim \mathcal{N}(0, \mathbf{I})$
 - 2: **for** $t = T, \dots, 1$ **do**
 - 3: $\mu, \Sigma \leftarrow \mu_\theta(x_t), \Sigma_\theta(x_t)$
 - 4: $\tilde{x}_0 \leftarrow \frac{1}{\sqrt{\alpha_t}} x_t - \frac{\sqrt{1-\alpha_t}}{\sqrt{\alpha_t}} \epsilon_\theta(x_t, t)$
 - 5: $\hat{y} \leftarrow \tilde{x}_0 * T + (1 - T) * A$
 - 6: $T \leftarrow T - l \nabla_T \mathcal{L}(y, \hat{y})$
 - 7: $g \leftarrow -\nabla_{\tilde{x}_0} \mathcal{L}(y, \hat{y})$
 - 8: Sample $x_{t-1} \sim \mathcal{N}(\mu + sg, \Sigma)$
 - 9: **end for**
 - 10: **return** x_0
-

Algorithm 4 Guidance on x_t and underwater image domain

Input: Underwater image y , global background light A , transmission map T , learning rate l for optimizing T , pre-trained diffusion model $(\mu_\theta(x_t), \Sigma_\theta(x_t))$, loss function \mathcal{L} , and gradient scale s

Output: Enhanced image x_0

- 1: $\hat{x} \leftarrow \text{Enhance}(y)$
 - 2: Sample $x_T \sim \mathcal{N}(0, \mathbf{I})$
 - 3: **for** $t = T, \dots, 1$ **do**
 - 4: $\mu, \Sigma \leftarrow \mu_\theta(x_t), \Sigma_\theta(x_t)$
 - 5: $\hat{y} \leftarrow x_t * T + (1 - T) * A$
 - 6: $T \leftarrow T - l \nabla_T \mathcal{L}(y, \hat{y})$
 - 7: $g \leftarrow -\nabla_{x_t} \mathcal{L}(y, \hat{y})$
 - 8: Sample $x_{t-1} \sim \mathcal{N}(\mu + sg, \Sigma)$
 - 9: **end for**
 - 10: **return** x_0
-

Algorithm 5 UIEDP algorithm with DDIM sampling strategy

Input: Underwater image y , any other UIE algorithm $\text{Enhance}(\cdot)$, pre-trained diffusion model $\epsilon_\theta(x_t, t)$, loss function \mathcal{L} , and gradient scale s

Output: Enhanced image x_0

- 1: $\hat{x} \leftarrow \text{Enhance}(y)$
 - 2: Sample $x_T \sim \mathcal{N}(0, \mathbf{I})$
 - 3: **for** $t = T, \dots, 1$ **do**
 - 4: $\tilde{x}_0 \leftarrow \frac{1}{\sqrt{\alpha_t}} x_t - \frac{\sqrt{1-\alpha_t}}{\sqrt{\alpha_t}} \epsilon_\theta(x_t, t)$
 - 5: $g \leftarrow -\nabla_{\tilde{x}_0} \mathcal{L}(\hat{x}, \tilde{x}_0)$
 - 6: $\hat{\epsilon} \leftarrow \epsilon_\theta(x_t, t) - \sqrt{1-\alpha_t} sg$
 - 7: $x_{t-1} \leftarrow \sqrt{\alpha_{t-1}} \left(\frac{x_t - \sqrt{1-\alpha_t} \hat{\epsilon}}{\sqrt{\alpha_t}} \right) + \sqrt{1-\alpha_{t-1}} \hat{\epsilon}$
 - 8: **end for**
 - 9: **return** x_0
-

C More ablations

In this section, we conducted more ablations to further validate the effectiveness of UIEDP.

Ablations about other UIE algorithms. In the main paper, we utilize UIEC²Net and Fusion as the algorithms responsible for generating pseudo-labeled images in UIEDP. We observe consistent improvements in image quality generated by UIEDP compared to the pseudo-labeled images. Consequently, we replace the algorithms generating pseudo-labeled images with MLLE and FA⁺Net to ascertain if this improvement persisted. The experimental results are presented in Table 6. Our findings indicate that irrespective of the UIE algorithm integrated into UIEDP, it consistently generates superior enhanced images, which further emphasizes the effectiveness of the diffusion prior.

Ablations about the variance Σ . During the conditional sampling process, we omitted one coefficient of gradient, i.e., the distribution variance Σ predicted by the diffusion model. According to the experimental results in Table 7, we find that the variance Σ negatively influences the generated images. Hence, we shift the mean by sg instead of $s\Sigma g$.

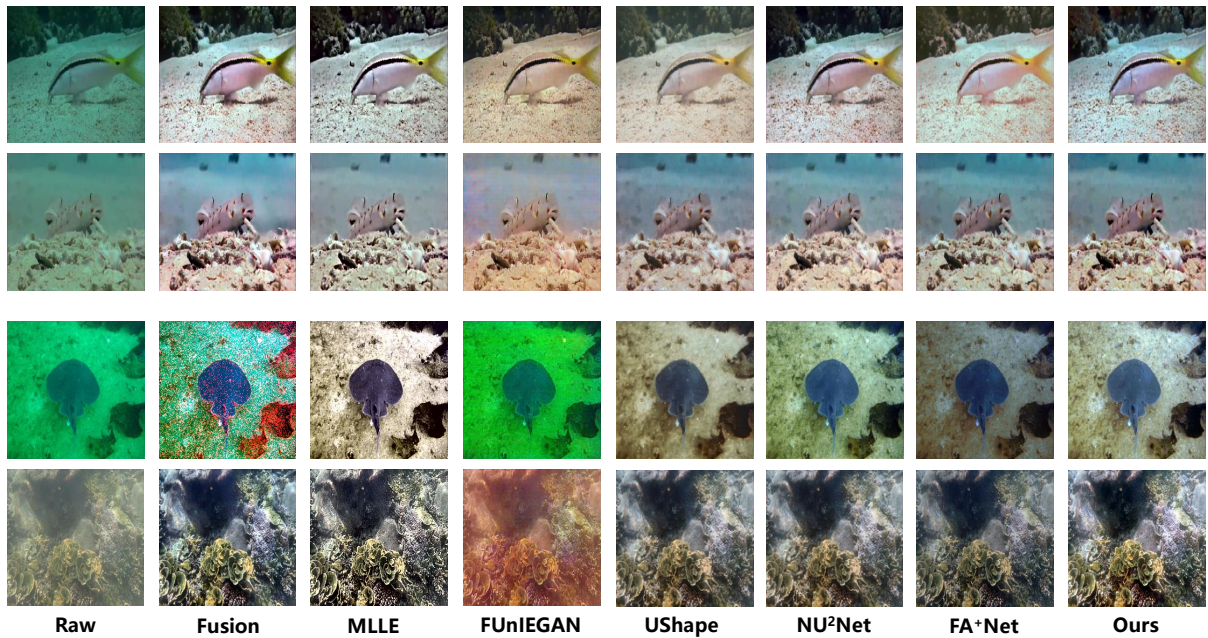


Figure 8: Visual comparison of different UIE methods on C60 and U45.

	PSNR \uparrow	SSIM \uparrow	UCIQE \uparrow	UIQM \uparrow	NIQE \downarrow
MLLE	19.48	0.84	0.60	2.45	4.87
UIEDP (MLLE)	19.91	0.85	0.60	2.53	4.65
FA ⁺ Net	20.98	0.88	0.59	2.92	4.83
UIEDP (FA ⁺ Net)	21.05	0.88	0.60	3.05	4.64

Table 6: Ablations about other UIE algorithms on T90.

	PSNR \uparrow	SSIM \uparrow	UCIQE \uparrow	UIQM \uparrow	NIQE \downarrow
with Σ	22.98	0.90	0.62	3.03	4.60
without Σ	23.44	0.91	0.63	3.13	4.54

Table 7: Ablations about the variance Σ on T90.

D More Visual Results

As shown in Figure 8, we present an intuitive comparison with other UIE methods in terms of visual effects. The first two rows are samples from C60, and the last two rows are samples from U45.